PHOTONICS Research

High-speed Stokes vector receiver enabled by a spin-dependent optical grating

Youpeng Xie,[1] Ting Lei,[1] Dawei Wang,[2] Jianxin Ren,[3] Yanmeng Dai,[1] Yanjun Chen,[2] Luping Du,[1] Bo Liu,[3,4] Zhaohui Li,[2,5] and Xiaocong Yuan[1,6]

[1]Nanophotonics Research Centre, Shenzhen University, Shenzhen 518060, China
[2]State Key Laboratory of Optoelectronic Material and Technologies and School of Electronics and Information Technology, Sun Yat-sen University, Guangzhou 510006, China
[3]Institute of Optics and Electronics, Nanjing University of Information Science and Technology, Nanjing 210044, China
[4]e-mail: bo@nuist.edu.cn
[5]e-mail: lzhh88@mail.sysu.edu.cn
[6]e-mail: xcyuan@szu.edu.cn

Received 7 December 2020; revised 9 March 2021; accepted 13 April 2021; posted 27 May 2021 (Doc. ID 416376); published 15 July 2021

Stokes vector direct detection is a promising, cost-effective technology for short-distance communication applications. Here, we design and fabricate a spin-dependent liquid crystal grating to detect light polarization states. By separating the circular and linear components of incident light, the polarization states can be resolved with accuracy of up to 0.25°. We achieved Stokes vector direct detection of quadrature phase-shift keying (QPSK), 8PSK, and 16-ary quadrature amplitude modulation signals with 32, 16, and 16 GBd rates, respectively. We integrated the system, including the grating, photodetectors, and optical elements, on a miniaturized printed circuit board and demonstrated high-speed optical communications with 16 GBd rate QPSK signals.

https://doi.org/10.1364/PRJ.416376

1. INTRODUCTION

With the development of big data, cloud computing, and 5G communications technology, increasingly large amounts of data are placing higher demands on our communication systems. Coherent optical transmission systems use more dimensions of light waves to achieve high spectral efficiency and high transmission rates [1–4]. Coherent optical communications can further improve both the total capacity and transmission distances of communication systems when combined with the original time division multiplexing [5,6] and wave division multiplexing systems [7,8]. The combination of coherent light detection and digital signal processing is already widely used in long-distance optical communications [9–11]. However, short-distance optical transmission and optical interconnection applications, such as data centers and 5G base stations, are more sensitive to the cost per bit and energy consumption [12,13]. There is tremendous demand for low-cost, high-speed, and high-capacity optical transmission. An alternative approach would be to return to direct detection optical transmission technology rather than using coherent solutions [14–19]. Direct detection has thus become a research hotspot in the high-speed optical transmission field in recent years.

Stokes vector direct detection is considered to be a power-efficient and low-cost method for optical communications [20–23]. Many works based on Stokes vector receivers have been proposed and demonstrated [24–26]. For example, a novel Stokes vector receiver with a 1×4 multimode interference power splitter has been used to demonstrate decoding of two-level pulse-amplitude modulation (PAM2) and four-level PAM (PAM4) signals at 3 GBd [24]. Each output arm of the Stokes vector receiver with on-chip photodetectors on a compact InP substrate contains an asymmetrical or symmetrical waveguide to convert the polarization. A monolithically integrated silicon photonic (SiPh) Stokes vector receiver demonstrated 128 Gb/s transmission over a 100-km-long single-mode fiber (SMF) [27]. The SiPh Stokes vector receiver needs six germanium photodetectors. However, waveguide based Stokes vector receivers are sensitive to temperature. They have large insertion losses of ~30 dB [24] and require complex fabrication technology [24,27]. An effective and flexible polarization demultiplexing scheme based on a Stokes analyzer has been demonstrated [28]. Using optical orthogonality monitoring and digital signal processing algorithms, polarization multiplexing signals can be demultiplexed adaptively after transmission for 10 km. The disadvantage of this work is that the polarization multiplexing degree has to be larger than 23°. Additionally, a modified signal with 16-ary quadrature amplitude modulation (16QAM) and PAM2 on two orthogonal polarizations was transmitted over a distance of 320 km using Stokes vector direct detection modulation and demodulation in a standard SMF [29]. Using a fully packaged InP in-phase/quadrature (IQ) modulator and a Stokes vector receiver that was realized using

discrete optics, the transmission of single-carrier 56 GBd 16-QAM, 8-QAM, and quadrature phase-shift keying (QPSK) optically modulated signals was demonstrated experimentally over distances of 320, 960, and 2880 km, respectively [30]. Although Stokes vector receivers that use a 90° hybrid [29] optical element or other discrete optics [30] have long transmission distances and high transmission rates, they are bulky in terms of physical size. As a summary, it is necessary to develop a Stokes vector receiver with low loss, temperature insensitivity, and miniaturized size. In our previous work, we achieved Stokes vector direct detection of QPSK, 8PSK, and 16QAM signals with 16, 8, and 4 GBd rates. The device was fabricated on a liquid crystal box. The liquid crystal box needs an applied voltage with square wave to control the half-wave condition of different central wavelengths [31].

In this paper, we design and fabricate a spin-dependent grating based on a liquid crystal polymer device with anisotropic periodic phase structures. The left-handed circular polarization (LCP), right-handed circular polarization (RCP), 0°, and 45° polarization components of the incident light are separated using the grating and detected to perform the Stokes vector measurements. Separating the circular and linear components of the incident light allows the polarization states to be resolved with accuracy of up to 0.3%. We demonstrate arbitrary polarization states detection using this miniaturized grating device with a performance comparable to that of a commercial Stokes analyzer. We use Stokes vector direct detection to achieve 32, 16, and 16 GBd rate optical transmissions. No additional polarization-tracking feedback circuit is required for the proposed system. We integrated the system including the grating, photodetectors, and optical elements on a miniaturized printed circuit board (PCB) with dimensions of 100 mm × 54.4 mm and demonstrated high-speed optical communications with 16 GBd rate QPSK signals.

2. PRINCIPLE OF THE SPIN-DEPENDENT GRATING

We design a spin-dependent optical grating with the Pancharatnam–Berry phase. This spin-dependent grating with its anisotropic periodic phase structure can detect the polarization components of light [32]. For a grating fabricated using isotropic materials (e.g., liquid crystals), the RCP light shows an opposite phase response. Therefore, this specially designed grating can separate the LCP and RCP components of the light. Figure 1(a) shows a schematic of the spin-dependent grating. A beam passing through the grating is diffracted into four orders that correspond to the LCP (−3rd order), original polarization (±1st orders), and RCP (+3rd order) components. We then place two polarizers at angles of 0° and 45° for the ±1st orders. Therefore, we obtain the intensities of the LCP, 0°, 45°, and RCP components of the polarized input light, which are sufficient to enable calculation of the four Stokes parameters and thus describe the polarized state of the light fully. Figure 1(b) shows the calculated grating structures along with two magnified pictures of the liquid crystal molecule distributions and their phase distributions for LCP light.

We fabricate the grating via photoalignment of a liquid crystal layer on a SiO_2 glass substrate with a thickness of 700 μm. These glass substrates are cleaned ultrasonically for several times. After they are dried in a drying oven and cleaned using ultraviolet (UV) light, the cleaned glass surfaces are rotation-coated with an optical alignment agent. The spin-coated optical alignment agent is 0.4% SD1 solvent. The glass surfaces with the SD1 solvent are then annealed on a hot stage at 100°C to volatilize the solvent. The processed glass can be exposed using 405 nm linearly polarized light. Using a digital micromirror device based digital mask lithography machine, we can then write the grating phase information into the device. Finally, we apply a liquid crystal polymer layer with a thickness that meets the half-wave condition and polymerize this layer under the action of UV light. This type of liquid crystal polymer device offers the advantage of stability, and can also be made to operate in different wavelength ranges near a central wavelength by changing the thickness of the polymer. A micrograph of the grating was captured by polarization microscopy and is shown in Fig. 1(b). The grating has an area of 2 mm × 1 mm with a

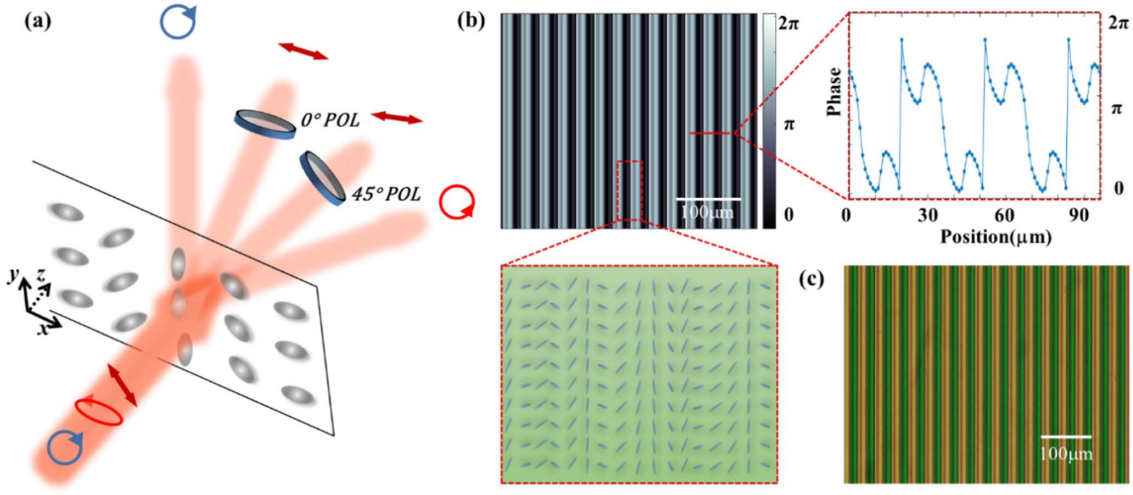

Fig. 1. Schematic and phase distribution of the spin-dependent grating for LCP light. (a) Schematic of the spin-dependent grating. (b) Calculated phase distribution of the spin-dependent grating along with two magnified pictures of the liquid crystal molecule distributions and their phase distributions. (c) Phase distribution of the spin-dependent grating under a polarizing microscope.

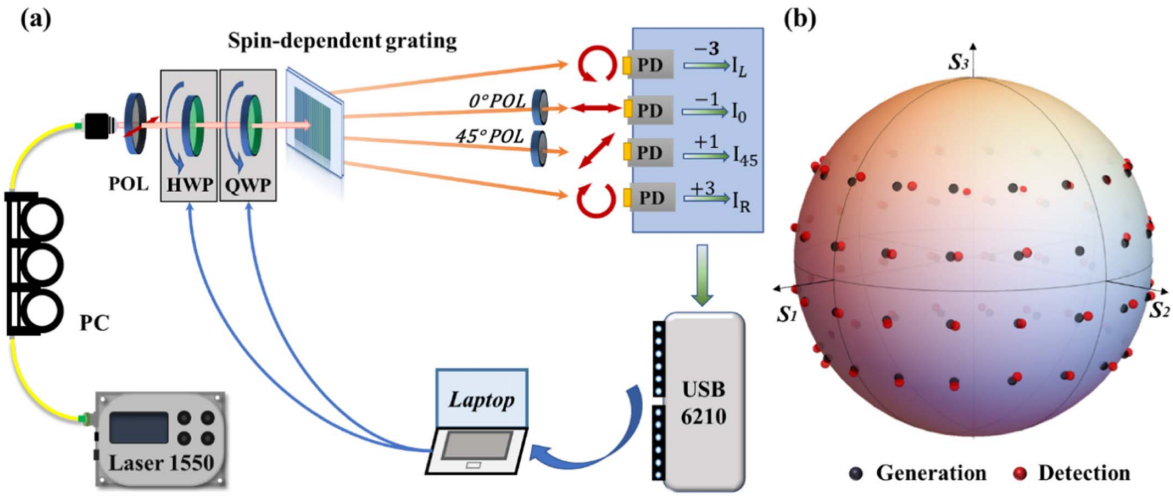

Fig. 2. (a) Setup for device characterization by measuring the arbitrary polarization states of light. (b) Experimental results for 72 sets of Stokes parameter measurements. PC, polarization controller; HWP, half-wave plate; QWP, quarter-wave plate; POL, polarizer; PD, photodetector.

pixel size of 1 μm and a grating period of 32 μm. The light efficiency is measured to be greater than 50%.

Figure 2(a) shows the setup used to perform device characterization by measuring arbitrary polarization states of light. A laser beam at a wavelength of 1550.11 nm is incident into free space via a collimator (Thorlabs F220APC-1550). The beam diameter is 2.1 mm. We add a polarization controller and a polarizer to the setup to ensure that the polarization direction is horizontal. By controlling the angles of a half-wave plate (HWP) and a quarter-wave plate (QWP) in combination, an arbitrary polarization state can be generated. The HWP and QWP are installed in two independently motorized precision rotation mounts (Thorlabs KPRM1E/M) to achieve precise rotations and obtain the desired polarization. The polarized light generated is diffracted for specific orders by the spin-dependent grating, and the LCP, 0°, 45°, and RCP components are detected using four photodetectors (Hamamatsu G12182-030K). The two motorized precision rotation mounts and four photodetectors are controlled using the LabVIEW program for motion synchronization and data accumulation. Therefore, the polarization state can be restored via Stokes calculations based on the intensities of the four components [33]. Figure 2(b) shows the experimental results for 72 sets of Stokes parameter measurements, where the black dots and the red dots indicate the generated and detected polarization states on a Poincaré sphere. We can describe the test results using a relative error value. The average of the relative errors of the n polarizations is given by

$$\sigma = \sum_{1}^{n} \frac{\sqrt{(s_1 - S_1)^2 + (s_2 - S_2)^2 + (s_3 - S_3)^2}}{n \times s_0}, \quad (1)$$

where n is the number of polarization states, s represents the theoretical values, and S represents the experimental values. In our experiment, we first rotate the HWP and QWP to generate linearly polarized light at different angles. The angle between two adjacent linearly polarized light beams is 0.25° with 720 states of polarization. We calculated that the σ value for these 720 polarization states is 0.3%. We also have a fixed HWP and rotate the QWP from 0° to 180°, thus generating a series of polarization states that include linear polarizations, circular polarizations, and elliptical polarizations. We also calculated that the σ value of these 720 polarization states is 0.4%. The experimental results show Stokes parameter accuracy comparable to that of commercial Stokes analyzers [34].

3. STOKES VECTOR DIRECT DETECTION EXPERIMENTS

The spin-dependent grating demonstrates good performance in detecting the polarization states of light. Using this liquid crystal grating, we can also achieve high-speed Stokes vector direct detection optical communication in combination with commercial high-speed photodetectors (Finisar MPRV1331A).

Figure 3 shows the Stokes communication system setup when using the spin-dependent grating as a receiver. A laser beam with power of 16 dBm at a wavelength of 1550.11 nm is incident into an optical multi-format transmitter (ID photonics OMFT) containing a dual-polarization IQ modulator through a polarization-maintaining fiber. A radio-frequency amplifier and a bias controller are integrated into the optical transmitter. The dual-polarization IQ modulator is driven using an arbitrary waveform generator (Keysight M8195A, 65 GSa/s) with four channels. To reduce cross talk between adjacent symbols, the digital baseband signals pass through a rising cosine pulse shaping filter that has a rolling coefficient of 0.35.

The dual-polarization IQ modulator has two orthogonal polarization directions. We can thus modulate different signals using these two orthogonal polarizations. QPSK, 8PSK, and 16QAM signals are generated with x polarization. Modified signals that act as a phase reference are generated with y polarization and phases of $\pi/4$ or $5\pi/4$ regularly [29].

The transmitted optical signals with x polarization and y polarization can be represented using the Jones vector

$$|E\rangle = [E_X, E_Y]', \quad (2)$$

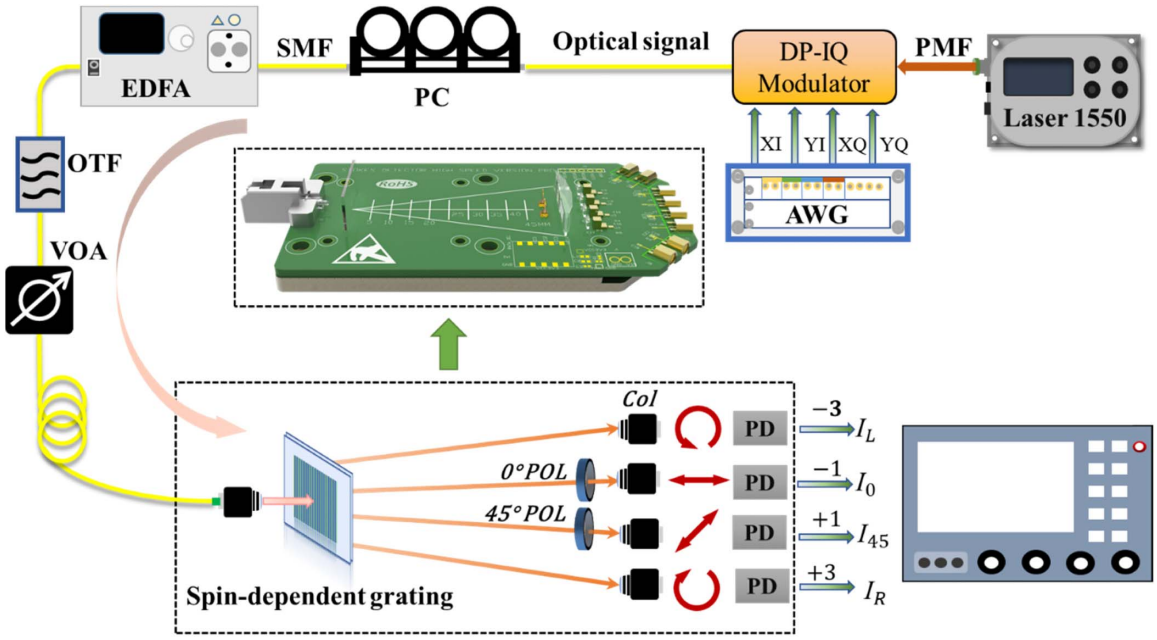

Fig. 3. High-speed Stokes optical communication system. PMF, polarization-maintaining fiber; DP-IQ modulator, dual-polarization in-phase/quadrature modulator; AWG, arbitrary waveform generator; SMF, single-mode fiber; PC, polarization controller; EDFA, erbium-doped fiber amplifier; OTF, optical tunable filter; VOA, variable optical attenuator; POL, polarizer; Col, collimator; PD, photodetector.

where E_X and E_Y are the transmitted complex fields for the two orthogonal polarizations, respectively. The modulated signals with different formats have different polarization distribution states in Stokes space. Using the Pauli matrix, we can then obtain the Stokes vector of this optical signal [35]:

$$S_i = \langle \boldsymbol{E}|\boldsymbol{\sigma}_i|\boldsymbol{E}\rangle = [E_X, E_Y] * \boldsymbol{\sigma}_i[E_X, E_Y], \quad i = 1, 2, 3. \tag{3}$$

As an example, Fig. 4 shows the normalized polarization state distributions of the 16QAM signals in Stokes space. There are three intensities (indicated by yellow, orange, and red colors).

The output beam from the transmitter is modulated with high-speed changes in their intensity and polarization. The optical signals from the transmitter are amplified using an erbium-doped fiber amplifier (EDFA) and then filtered using a tunable optical filter (Santec OTF-350). The optical output power is controlled using a variable optical attenuator. After being transmitted for more than 10 m in a standard SMF, the signals are demodulated using the Stokes vector receiver, which includes the liquid crystal grating, two polarizers, and four photodetectors. The total power loss of the free space setup is 8 dB. The changes in light intensities of the different signals are converted into electrical signals by the photodetectors and sampled using an oscilloscope with four channels (Agilent DSAX93204A, 80 GSa/s) in real time.

The light intensity data sampled using the oscilloscope can be processed offline using an algorithm in MATLAB. The data from these four channels are then correlated with

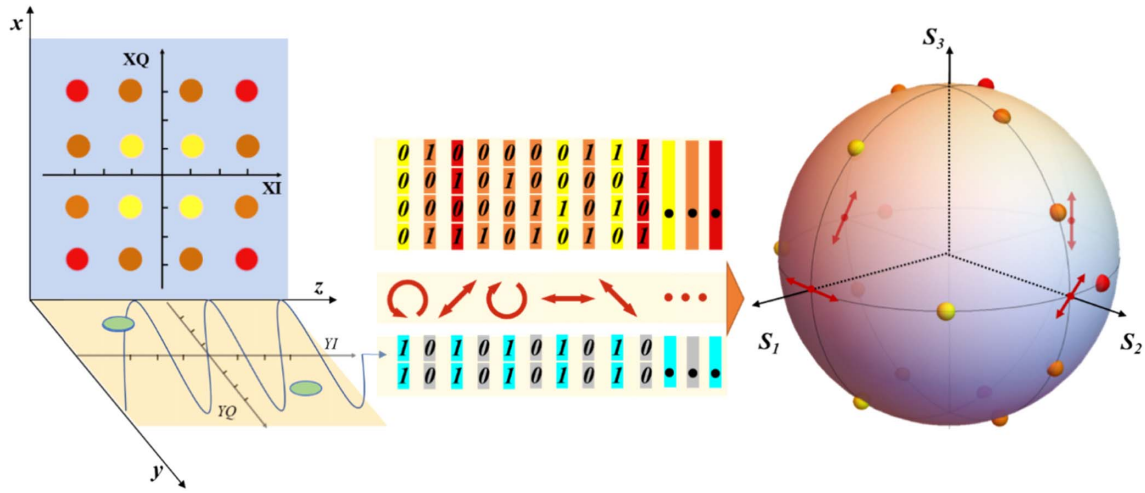

Fig. 4. Normalized polarizations of the 16QAM signals in the Stokes space.

the transmitted Stokes signals. After cross-correlation synchronization and resampling, each polarization state then corresponds to a unique set of light intensities. However, after transmission of the optical signals in free space and in an optical fiber, the induced losses and the rotation of the polarization states will affect the calculation results. In an SMF, the light polarization state is unstable because of external mechanical factors, e.g., bending, twisting, vibration, and compression [36]. We can compensate for these effects using a transmission matrix [37]. This matrix changes with the optical communication system in real time. The received Stokes vector can then be calculated as follows:

$$\begin{bmatrix} S_0 \\ S_1 \\ S_2 \\ S_3 \end{bmatrix} = \begin{bmatrix} m_{11} & m_{12} & m & m_{14} \\ m_{21} & m_{22} & m_{23} & m_{24} \\ m_{31} & m_{32} & m_{33} & m_{34} \\ m_{41} & m_{42} & m_{43} & m_{44} \end{bmatrix} \begin{bmatrix} I_l \\ I_{0^\circ} \\ I_{45^\circ} \\ I_r \end{bmatrix}. \quad (4)$$

To calculate the Stokes vector, we first need to calibrate the transmission matrix using known polarization states. In the high-speed communication system, we generate 64 different polarization state types by controlling the input signals in the x and y directions of the dual-polarization modulator. After transmission of the training signals is repeated 32 times, we can then extract the matrix for the received data. We then use 20,480 symbols of random QPSK/8PSK/16QAM signals in the x direction and reference signals in the y direction to generate the optical signals for Stokes communication.

The retrieved Stokes vectors on the Poincaré sphere for 32 GBd QPSK, 16 GBd 8PSK, and 16 GBd 16QAM signals are shown in Fig. 5(a).

Furthermore, we can calculate the Jones vector from each obtained Stokes vector as follows [35]:

$$|E\rangle = C\begin{pmatrix} \sqrt{1/2(S_0+S_1)} \\ \sqrt{1/2(S_0-S_1)}\exp[i\cdot\arctan(S_3/S_2)] \end{pmatrix}. \quad (5)$$

Here, although the complex constant C is variable, the x- and y-polarized components of the Jones vector have fixed phase differences. We use the y-polarized component as the phase reference, and demodulate the QPSK/8PSK/16QAM signals on the x polarization with a least mean squares equalizer. We extract the intensity and phase of the input signals, and obtain constellation diagrams, as shown in Fig. 5(b).

We measure the bit error rate (BER) curves of the different modulation formats for various received powers. Figure 5(c) shows the BER curves of the 32 GBd QPSK, 16 GBd 8PSK, and 16 GBd 16QAM signals. The BERs of all the above modulation formats meet the requirements of the 20% hard-decision forward error correction threshold. The BER curve of the QPSK signals at the 32 GBd rate shows better performance than the curves of the other modulation formats. The BER of the QPSK signals decreases with increasing received power and reaches zero when the received power is greater than 4 dBm. The BER of the 8PSK signal is better than 16QAM signal. The spin-dependent optical grating shows a wideband response. We also measured the BER curves of the 32 GBd QPSK, 16 GBd 8PSK, and 16 GBd 16QAM signals with different wavelengths

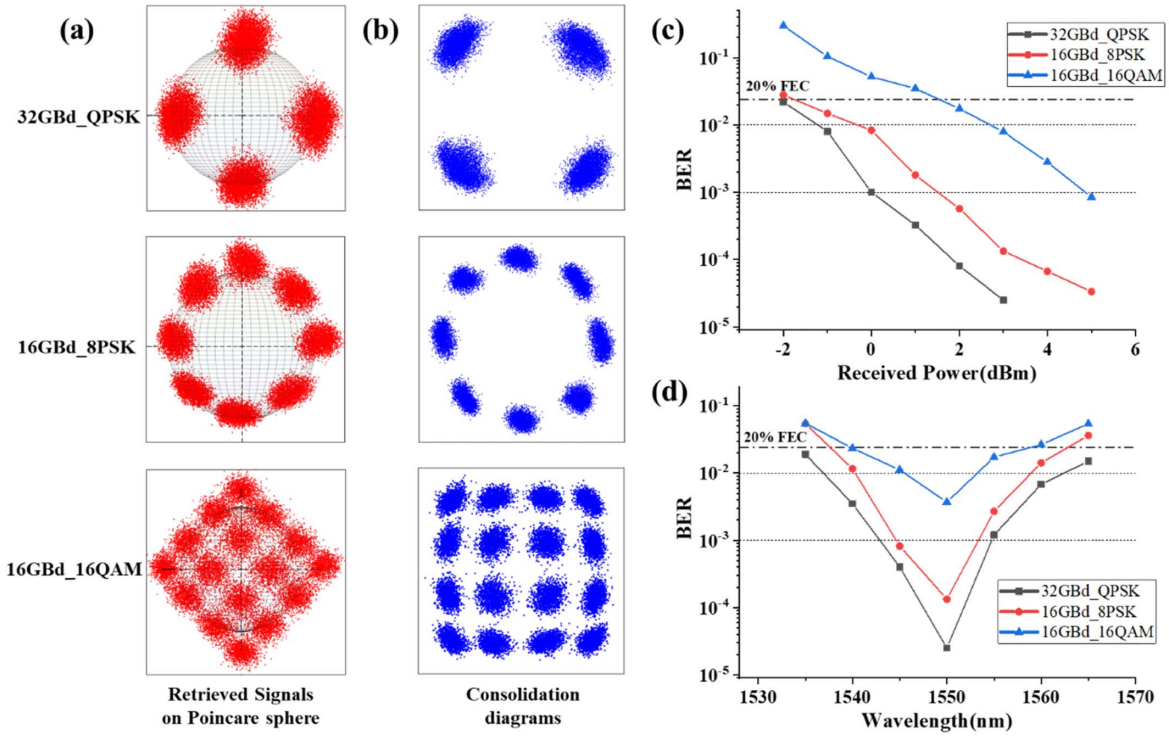

Fig. 5. Stokes communication when using the spin-dependent grating as a receiver. (a) Plots of retrieved Stokes vectors on the Poincaré sphere for 32 GBd QPSK, 16 GBd 8PSK, and 16 GBd 16QAM signals. (b) Corresponding constellation diagrams for the vectors in (a). (c) Bit error rate (BER) curves of the 32 GBd QPSK, 16 GBd 8PSK, and 16 GBd 16QAM signals with received power. (d) BER curves of the 32 GBd QPSK, 16 GBd 8PSK, and 16 GBd 16QAM signals with different wavelengths.

within the C-band. The wavelength interval used was 5 nm over the range from 1535 to 1565 nm. Figure 5(d) shows the BER curves of the 32 GBd QPSK, 16 GBd 8PSK, and 16 GBd 16QAM signals with a power of 3 dBm. The BERs show minimum values at the central wavelength of the C-band. This is because the diffraction angle of the grating varies with the operating wavelength. Changes in the diffraction angle induce coupling loss to the photodetectors.

The initial experiment was based on an optical platform composed of discrete components. We then integrated the Stokes communication system onto a 100 mm × 54.4 mm PCB, as shown in the center image of Fig. 3. Light beams carrying the high-speed signals are incident via a fiber collimation head with a pluggable Lucent connector interface. The grating is fixed on the PCB. The collimated light is also diffracted into four beams through the grating. These four beams are then collimated using a specially designed lenticular lens. The total power loss of the integrated approach is 9 dB. The light intensity changes in the four beams are subsequently converted into changes in electrical currents. These current changes are amplified linearly using four transimpedance amplifiers (MACOM MATA-03003/3013B). The typical bandwidth is 21 GHz, and the typical noise current is 1.4 μA. These transimpedance amplifiers have differential outputs, and the background noise of each path can be eliminated by subtraction of two ports with differential outputs. Additionally, we placed a steel plate below the PCB and screwed the PCB onto the plate to reduce optical path drift. We also demonstrated high-speed optical communication with a 16 GBd rate QPSK signal. The integrated transmission system shows excellent communication performance with a BER of 4.7×10^{-3}.

4. CONCLUSION

In this work, we have designed a spin-dependent grating based on the Pancharatnam–Berry phase to detect the polarization states of light. A light beam that passes through the grating is diffracted into four orders. We placed two polarizers at angles of 0° and 45° for the −1st order and the +1st order, respectively. The four output beams correspond to the LCP, 0°, 45°, and RCP components of the input polarized light. By measuring the intensities of these components, we can then obtain the Stokes vector of the input light beam using a transmission matrix. The polarization states can be resolved with accuracy of up to 0.3%. We demonstrated the detection of arbitrary polarization states using this miniaturized grating device with a detection performance comparable to that of a commercial Stokes analyzer. We fabricated the grating on a liquid crystal polymer. This type of liquid crystal polymer device demonstrated stable performance. The grating can operate in different wavelength ranges near a central wavelength by simply varying the thickness of the polymer. We also achieved Stokes vector direct detection communication of QPSK, 8PSK, and 16QAM signals with 32, 16, and 16 GBd rates, respectively, using discrete optical elements. In addition, we integrated the system, including the grating, photodetectors, and optical elements, on a miniaturized PCB with dimensions of 100 mm × 54.4 mm. We then demonstrated high-speed optical communication with 16 GBd rate QPSK signals using the miniaturized Stokes vector receiver. The spin-dependent grating offers the advantages of compact size, low cost, and high efficiency for Stokes vector direct detection in optical communication systems.

Funding. National Key Research and Development Program of China (2018YFB1800901, 2018YFB1801801); National Natural Science Foundation of China (11774240, 61822507, 61935013, U1701661, U2001601); Science, Technology and Innovation Commission of Shenzhen Municipality (KQTD2015071016560101, KQTD20170330110444030).

Disclosures. The authors declare no conflicts of interest.

REFERENCES

1. G. Li, "Recent advances in coherent optical communication," Adv. Opt. Photon. **1**, 279–307 (2009).
2. K. Kikuchi, "Coherent optical communications: historical perspectives and future directions," in *High Spectral Density Optical Communication Technologies*, M. Nakazawa, K. Kikuchi, and T. Miyazaki, eds. (Springer Berlin Heidelberg, 2010), pp. 11–49.
3. M. Nakazawa, "Ultrahigh spectral density coherent optical transmission technologies," in *High Spectral Density Optical Communication Technologies*, M. Nakazawa, K. Kikuchi, and T. Miyazaki, eds. (Springer Berlin Heidelberg, 2010), pp. 51–80.
4. P. J. Winzer, "High-spectral-efficiency optical modulation formats," J. Lightwave Technol. **30**, 3824–3835 (2012).
5. D. O. Otuya, K. Kasai, T. Hirooka, and M. Nakazawa, "Single-channel 1.92 Tbit/s, 64 QAM coherent Nyquist orthogonal TDM transmission with a spectral efficiency of 10.6 bit/s/Hz," J. Lightwave Technol. **34**, 768–775 (2016).
6. M. Nakazawa, T. Hirooka, P. Ruan, and P. Guan, "Ultrahigh-speed "orthogonal" TDM transmission with an optical Nyquist pulse train," Opt. Express **20**, 1129–1140 (2012).
7. A. Sano, E. Yamada, H. Masuda, E. Yamazaki, T. Kobayashi, E. Yoshida, Y. Miyamoto, R. Kudo, K. Ishihara, and Y. Takatori, "No-guard-interval coherent optical OFDM for 100-Gb/s long-haul WDM transmission," J. Lightwave Technol. **27**, 3705–3714 (2009).
8. H. Rohde, E. Gottwald, A. Teixeira, J. D. Reis, A. Shahpari, K. Pulverer, and J. S. Wey, "Coherent ultra dense WDM technology for next generation optical metro and access networks," J. Lightwave Technol. **32**, 2041–2052 (2014).
9. X. Zhou and L. Nelson, "Advanced DSP for 400 Gb/s and beyond optical networks," J. Lightwave Technol. **32**, 2716–2725 (2014).
10. A. Leven, N. Kaneda, and S. Corteselli, "Real-time implementation of digital signal processing for coherent optical digital communication systems," IEEE J. Sel. Top. Quantum Electron. **16**, 1227–1234 (2010).
11. S. J. Savory, "Digital signal processing for coherent optical communication systems," in *Optoelectronics & Communications Conference Held Jointly with International Conference on Photonics in Switching* (2013), paper TuR3_1.
12. L. Tao, Y. Ji, J. Liu, A. P. T. Lau, N. Chi, and C. Lu, "Advanced modulation formats for short reach optical communication systems," IEEE Netw. **27**, 6–13 (2013).
13. K. Zhong, X. Zhou, J. Huo, C. Yu, C. Lu, and A. P. T. Lau, "Digital signal processing for short-reach optical communications: a review of current technologies and future trends," J. Lightwave Technol. **36**, 377–400 (2018).
14. M. Schuster, S. Randel, C. A. Bunge, S. C. J. Lee, F. Breyer, B. Spinnler, and K. Petermann, "Spectrally efficient compatible single-sideband modulation for OFDM transmission with direct detection," IEEE Photon. Technol. Lett. **20**, 670–672 (2008).
15. D. Che, A. Li, X. Chen, Q. Hu, Y. Wang, and W. Shieh, "160-Gb/s stokes vector direct detection for short reach optical communication," in *Optical Fiber Communication (OFC) Conference* (2014), pp. 1–3.

16. H. Khodakarami, D. Che, and W. Shieh, "Information capacity of polarization-modulated and directly detected optical systems dominated by amplified spontaneous emission noise," J. Lightwave Technol. **35**, 2797–2802 (2017).
17. H. Chen, J. C. Alvarado-Zacarias, H. Huang, N. K. Fontaine, R. Ryf, D. T. Neilson, and R. Amezcua-Correa, "Mode-multiplexed full-field reconstruction using direct and phase retrieval detection," in *Optical Fiber Communication Conference* (2020), paper W4A.5.
18. M. Chagnon, M. Morsy-Osman, and D. V. Plant, "Multi-dimensional formats and transceiver architectures for direct detection with analysis on inter-polarization phase modulation," J. Lightwave Technol. **35**, 885–892 (2017).
19. Y. Zhu, B. Yang, Y. Zhong, Z. Liu, and Z. Ma, "Performance comparison of coherent and direct detection schemes for 50G PON," in *Optical Fiber Communication Conference* (2020), paper W1E.3.
20. W. Shieh, A. Li, D. Che, F. Yuan, and H. Khodakarami, "Stokes-vector direct detection for optical communications," Proc. SPIE **10130**, 101300G (2017).
21. W. Shieh and D. Che, "Optical field recovery via Stokes vector direct detection," in *Optical Fiber Communication Conference* (2019), paper M1H.1.
22. A. Singh, "Stokes vector-based polarization management in optical communication system: a review," Opt. Eng. **59**, 090901 (2020).
23. L. Cheng, L. Xi, D. Zhao, X. Tang, W. Zhang, and X. Zhang, "Improved modulation format identification based on Stokes parameters using combination of fuzzy c-means and hierarchical clustering in coherent optical communication system," Chin. Opt. Lett. **13**, 100604 (2015).
24. S. Ghosh, T. Tanemura, Y. Kawabata, K. Katoh, K. Kikuchi, and Y. Nakano, "Decoding of multilevel Stokes-vector modulated signal by polarization-analyzing circuit on InP," J. Lightwave Technol. **36**, 187–194 (2018).
25. T. Suganuma, S. Ghosh, M. Kazi, R. Kobayashi, Y. Nakano, and T. Tanemura, "Monolithic InP Stokes vector receiver with multiple-quantum-well photodetectors," J. Lightwave Technol. **36**, 1268–1274 (2018).
26. A. Li, S. Chowdhury, Y. Wen, W.-R. Peng, Y. Cui, and Y. Bai, "112 Gb/s self-heterodyne Stokes vector detection with compact receiver for short reach optical communications," in *Optical Fiber Communication Conference* (2018), paper W1J.1.
27. P. Dong, X. Chen, K. Kim, S. Chandrasekhar, Y.-K. Chen, and J. H. Sinsky, "128 Gb/s 100-km transmission with direct detection using silicon photonic Stokes vector receiver and I/Q modulator," Opt. Express **24**, 14208–14214 (2016).
28. Z. Chen, L. Yan, W. Pan, B. Luo, A. Yi, Y. Pan, L. Jiang, J. Ye, X. S. Yao, and G. Li, "A highly flexible polarization demultiplexing scheme for short-reach transmission," IEEE Photon. J. **7**, 7905108 (2015).
29. T. Hoang, M. Sowailem, Q. Zhuge, M. Osman, A. Samani, C. Paquet, S. Paquet, I. Woods, and D. Plant, "Enabling high-capacity long-reach direct detection transmission with QAM-PAM Stokes vector modulation," J. Lightwave Technol. **36**, 460–467 (2018).
30. M. Y. S. Sowailem, T. M. Hoang, M. Chagnon, M. Morsy-Osman, M. Qiu, S. Paquet, C. Paquet, I. Woods, O. Liboiron-Ladouceur, and D. V. Plant, "100G and 200G single carrier transmission over 2880 and 320 km using an InP IQ modulator and Stokes vector receiver," Opt. Express **24**, 30485–30493 (2016).
31. Y. Xie, T. Lei, H. Ye, Y. Chen, D. Wang, Y. Dai, L. Du, Z. Li, and X. Yuan, "Stokes vector direct detection using a spin-dependent grating," in *Asia Communications and Photonics Conference/International Conference on Information Photonics and Optical Communications (ACP/IPOC)* (2020), paper S3H.1.
32. Y. Dai, Y. Zhang, Y. Xie, D. Wang, X. Wang, T. Lei, C. Min, and X. Yuan, "Multifunctional geometric phase optical element for high-efficiency full Stokes imaging polarimetry," Photon. Res. **7**, 1066–1074 (2019).
33. R. M. A. Azzam and A. G. Lopez, "Accurate calibration of the four-detector photopolarimeter with imperfect polarizing optical elements," J. Opt. Soc. Am. A **6**, 1513–1521 (1989).
34. Thorlabs, "Polarimeter systems with high dynamic range," https://www.thorlabschina.cn/newgrouppage9.cfm?objectgroup_id=1564 (2020).
35. J. N. Damask, *Polarization Optics in Telecommunications* (Springer, 2005).
36. G. Agrawal, *Applications of Nonlinear Fiber Optics* (Elsevier, 2020).
37. D. Che and W. Shieh, "Polarization demultiplexing for Stokes vector direct detection," J. Lightwave Technol. **34**, 754–760 (2016).